POST-BEAMFORMING THIRD-ORDER VOLTERRA FILTER (THOVF) FOR PULSE-ECHO ULTRASONIC IMAGING

Mamoun F. Al-Mistarihi, Pornchai Phukpattaranont and Emad S. Ebbini
Department of Electrical and Computer Engineering, University of Minnesota, Minneapolis, MN 55455
{mamoun, pornchai, emad @ece.umn.edu}

ABSTRACT

A ThOVF is applied to separate linear, quadratic, and cubic components from beamformed ultrasonic pulse-echo imaging data from nonlinear media. In the context of imaging ultrasound contrast agents (UCAs) infused in tissue media, the ThOVF offers the advantage of essentially complete separation of the nonlinear responses of the UCAs and tissues (since the latter rarely produces higher than quadratic nonlinear response). We describe an SVD-based robust algorithm for estimating the coefficients of the ThOVF from beamformed data. In addition, experimental results from imaging of UCA in flow channels through tissue-mimicking phantoms demonstrate the advantage of this approach. We show imaging results with computed contrast-to-tissue ratio (CTR), histograms of UCA and tissue regions, and average spectra from UCA and tissue region. These results individually and collectively support the hypothesis that ThOVF is the appropriate model for complete separation of nonlinear echoes from UCA and tissue.
.

1. INTRODUCTION

We have previously validated the applicability of a second-order Volterra filter (SOVF) model for decomposing the pulse-echo ultrasonic radio-frequency (RF) signal into its linear and quadratic components [3]. A post-beamforming SOVF was shown to significantly improve the CTR and improve the dynamic range of ultrasonic imaging. This post-beamforming SOVF was shown to achieve comparable performance to pulse inversion method described in [5], currently considered the most sensitive to the presence of nonlinear echoes due to microbubble contrast agents for ultrasonic imaging. In pulse inversion (PI) imaging, a sequence of two inverted acoustic pulses with appropriate delay is transmitted into tissue. Images are produced by summing the corresponding two backscattered signals. The PI imaging overcomes the tradeoff between contrast and spatial resolution because it utilizes the entire bandwidth of the backscattered signals. As a result, superior spatial resolution can be achieved when compared with simplistic second harmonic (SH) imaging. The cost of this enhanced performance, however, is a reduction of the image frame rate. This severely limits the use of this method in some critical application areas such as cardiology. On the other hand, the SOVF does not require multiple transmissions to form the image. Currently, the main limitation of the SOVF is that the quadratic component of the echo signal does not completely separate the tissue nonlinearity from the contrast nonlinearity, thus limiting its ability to achieve maximum contrast.

In this paper, a postbeamforming nonlinear filter based on the third-order Volterra filter (ThOVF) is presented. The filter is capable of separating linear, quadratic and cubic components from beamformed backscattered signals. The motivation for this approach is that, while ultrasonic propagation in tissue is fundamentally nonlinear, this nonlinearity is not higher than quadratic. On the other hand, echoes from UCA typically produce cubic and even higher nonlinearity. Therefore, the ThOVF has the potential of contrast enhancement at levels equal or greater than those achieved by PI imaging. In what follows, we describe an algorithm for estimating the model coefficients from the beamformed data and the application of the cubic filter to produce images of the cubic images. Comparisons with standard ultrasonic images based on the unfiltered RF data are made in addition to comparison with images from PI and quadratic imaging to demonstrate the usefulness of the ThOVF approach.

2. THEORY

In this section, the decomposition of received echo, i.e., output sequence only, into linear, quadratic, and cubic components by using least-squares approach of third-order Volterra model is considered. The details of algorithm implementation to pulse-echo ultrasound imaging are stated.

2.1 System Identification

The algorithm in this section is adapted from [6], which has shown the validity of a SOVF as a model for pulse-echo ultrasound data. The response of a cubically nonlinear system $y(n+1)$, can be predicted by a third order Volterra model of m past values as follows:

$$\begin{aligned} y(n+1) &= \sum_{i=0}^{m-1} y(n-i)h_L(i) \\ &+ \sum_{i=0}^{m-1}\sum_{j=i}^{m-1} y(n-i)y(n-j)h_Q(i,j) \\ &+ \sum_{i=0}^{m-1}\sum_{j=i}^{m-1}\sum_{k=j}^{m-1} y(n-i)y(n-j)y(n-k)h_C(i,j,k) \end{aligned} \tag{1}$$

where $h_L(i)$, $h_Q(i,j)$ and $h_C(i,j,k)$ are the linear, quadratic and cubic filter coefficients respectively. It is easy to see that

(1) is a nonlinear equation in terms of the input. However, it is a linear equation in terms of the unknown filter coefficients (i.e., linear, quadratic and cubic Volterra kernels) $h_L(i)$, $h_Q(j,k)$ and $h_C(i,j,k)$. Hence, (1) was rewritten in vector form:

$$y(n+1) = Y^T(n)H \tag{2}$$

where past data vector $Y(n)$ is defined at time n as:

$$\begin{aligned} Y(n) = [&y(n), y(n-1), y(n-2), \ldots\ldots, y(n-m+1), \\ &y^2(n), y(n)y(n-1), \ldots\ldots, y^2(n-m+1), \\ &y^3(n), y^2(n)y(n-1), \ldots\ldots, y^3(n-m+1)]^T \end{aligned}$$

and the filter coefficient vector H is defined as:

$$\begin{aligned} H = [&h_L(0), h_L(1), h_L(2), \ldots\ldots, h_L(m-1), \\ &h_Q(0,0), h_Q(0,1), \ldots\ldots, h_Q(m-1, m-1) \\ &h_C(0,0,0), h_C(0,0,1), \ldots\ldots, h_C(m-1, m-1, m-1)]^T \end{aligned}$$

Note that m is the system order, N is the total number of filter coefficients, which is equal to

$$N = \frac{m^3 + 6m^2 + 11m}{3!}$$

assuming symmetrical quadratic and cubic kernels, and superscript ^{T} is the transpose of a vector or a matrix. A system of linear equations are formed in order to find filter coefficients as follows:

$$F = GH \tag{3}$$

where the vector F and the matrix G are

$$F = [y(n+1), y(n+2), \ldots\ldots, y(n+L)]^T$$

$$G = [Y(n), Y(n+1), \ldots\ldots, Y(n+L-1)]^T$$

A minimum norm least squares (MNLS) solution can be obtained by

$$H_{MNLS} = G^+F \tag{4}$$

where G^+ is generalized inverse. Assuming G has rank $r \le L$, the *SVD* of G can be expressed as

$$G = U\Sigma V^T = \sum_{i=1}^{r} \sigma_i u_i v_i^T \tag{5}$$

where Σ is a $L \times N$ diagonal matrix with singular values $\sigma_1 \ge \sigma_2 \ge \cdots \ge \sigma_r > \sigma_{r+1} = \cdots = \sigma_L = 0$, U and V are unitary matrices, and u_i and v_i are the orthogonal eigenvectors of GG^T and G^TG, respectively.

The SVD of G forms a basis for regularization by appropriate selection of singular modes that enhance the reconstructed image. A criterion for choosing these singular modes is needed. In the context of contrast agent imaging, an obvious criterion is the contrast-to-tissue ratio (*CTR*) given by:

$$CTR = 10\log_{10}\left(\frac{\overline{P_C}}{\overline{P_T}}\right), \tag{6}$$

where $\overline{P_C}$ and $\overline{P_T}$ are the l_2 norms of the cubic components from the contrast and normal tissue regions, respectively. The average power of signals in a given region, $\overline{P}$, can be expressed as

$$\overline{P} = \frac{1}{IJ}\left(\sum_{i=1}^{I}\sum_{j=1}^{J} x_{ij}^2\right) \tag{7}$$

where x_{ij} is the signal in that region. Note that the *CTR* used in this algorithm is determined from cubic components of the ThOVF model.

2.2 Cubic Images

Cubic images are obtained from cubic components of the third-order Volterra model. The coefficients of the ThOVF are derived from the beamformed RF data taken from a representative region on a standard B-mode image as follows. From the standard B-mode image, after a UCA region and a tissue region are defined for the *CTR* computation, a segment of RF data from an axial line is selected to form a system of linear equations. The SVD of the G matrix is computed, the filter coefficients for each singular mode of the G matrix are determined and the corresponding *CTRs* are computed. The cubic image is produced by applying the cubic filter coefficients of the singular mode of the G matrix that give the maximum *CTR* to the beamformed RF data throughout the standard B-mode image to estimate the cubic component

$$\hat{y}_C(n+1) = \sum_{i=0}^{m-1}\sum_{j=i}^{m-1}\sum_{k=j}^{m-1} y(n-i)y(n-j)y(n-k)\hat{h}_C(i,j,k) \tag{8}$$

where $\hat{h}_C(i,j,k)$ is the estimated cubic kernel. A flowchart of this algorithm is shown in Fig. 1.

3. MATERIALS AND METHODS

3.1 Contrast Agent

The contrast agent, BR14 (Bracco Research S.A., Geneva, Switzerland), was used. BR14 is a new experimental agent that consists of high molecular weight gas bubbles encapsulated by a flexible phospholipids shell. A 0.005 mL sample of 0.25 mL of BR14, prepared with 5 mL of 0.9% saline, was diluted in 500 mL of 0.9% saline leading to a 1:100000 dilution.

3.2 Imaging Target

A flow phantom (Model 524; ATS Laboratories, Inc., Bridgeport, CT) containing four flow channels with diameters 2, 4, 6, and 8 mm embedded in rubber-based tissue mimicking material was used in obtaining the images. The flow phantom was connected to a flow system with a roller pump (Model 77200-60; Cole-Parmer Instrument Co., Vernon Hills, IL). Subsequently, the diluted BR14 was circulated. In addition, the diluted BR14 was constantly stirred in a beaker using a magnetic hot plate stirrer (EW-84303-20; Corning Inc., Corning NY). This experiment was designed to compare B-mode, PI, quadratic, and cubic images of the nonlinear backscattered signals from BR14 in the 6 mm diameter flow channel. RF data were recorded and saved for later processing by the Technos MP ultrasound system (ESAOTE S.p.A, Genova, Italy) with a convex array probe (CA421; ESAOTE S.p.A, Genoa, Italy) located perpendicularly to the ultrasound contrast agent flow channel. A pair of 3-cycle inverted pulses at 1.56 MHz were transmitted to produce a PI image.

4. RESULTS AND DISCUSSION

Fig. 2 shows images obtained using standard B-mode, PI, quadratic image from 201st singular mode, and cubic image from 48th singular mode respectively. Each image shows the UCA in the 6-mm flow channel (left) and the 4-mm empty flow channel (right) surrounded by tissue-mimicking material. Due to differences in dynamic ranges, each image is displayed with its full dynamic range as can be seen from the dB-level scale bars. One can see that important regions of interest (UCA, tissue and empty flow channel regions) provide different levels of backscattered signals.

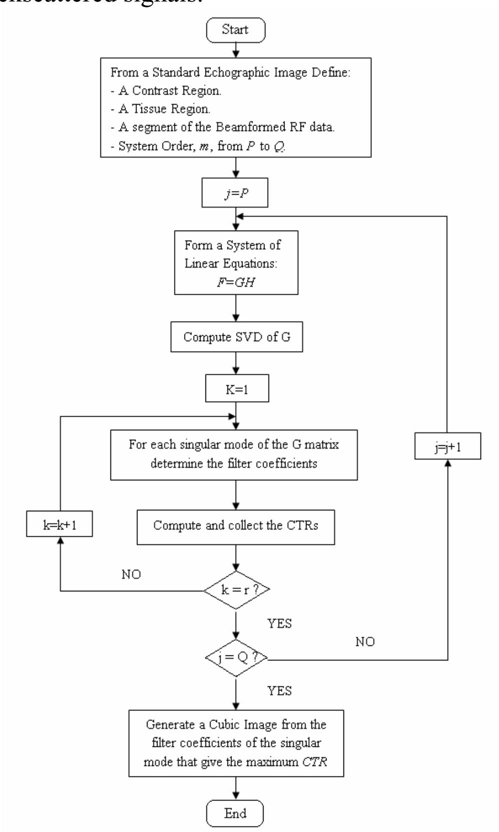

Fig.1 A flowchart of cubic image generation algorithm

The standard B-mode image provides *CTR* 4.8 dB whereas the PI image provides *CTR* 18.9 dB, which shows a contrast enhancement over the standard B-mode image. However, one can observe loss of signals from tissue and the empty flow channel due to the cancellation of linear components. The quadratic image from the 201st singular mode provides *CTR* 24.2 dB, which shows a contrast enhancement over both standard B-mode and PI images.

The cubic image from the 48th singular mode was obtained using the algorithm described by the flowchart of Figure 1, provides *CTR* 42.1 dB. This value indicates contrast enhancement over the standard B-mode, PI, and quadratic images. Moreover, it can be seen that contrasts are enhanced without loss of spatial resolutions. One important feature of the cubic image is the increased dynamic range compared to standard B-mode, PI and quadratic images. This increased dynamic range results in contrast enhancement without loss in image features such as specular reflections, which may be of diagnostic value in some cases.

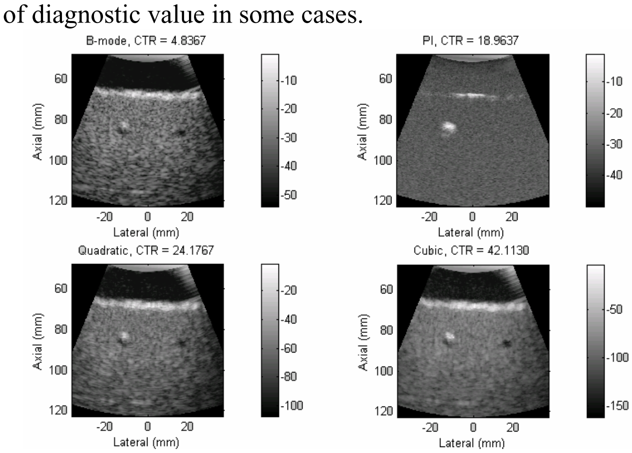

Fig. 2 Images of the flow phantom: Standard B-mode, PI, Quadratic from 201st Singular mode, and Cubic from 48th Singular mode.

Also, the speckle in the tissue region of the cubic image is finer than that of the standard B-mode and quadratic images. In addition to the contrast enhancement achieved by the cubic image, one can see that the empty flow channel is more visible than that in the standard B-mode, PI, and quadratic images. CTR values, axial and lateral resolution for the flow phantom are summarized in Table I. Axial and lateral resolution from PI images is not possible due to complete cancellation of speckle components in tissue region.

Table I

CTR, Axial resolution, and Lateral resolution for the three different imaging methods

Imaging method	CTR	Axial resolution	Lateral resolution
B-mode	4.8	1.34	1.66
Quadratic	24.2	1.03	1.50
Cubic	42.1	0.87	1.34

Fig. 3 shows the gray-level histograms produced from the Standard B-mode, PI, quadratic, and cubic images. In each case, the histogram from the UCA region is plotted with light solid line, while the histogram from tissue is plotted with darker solid line. One can see the degree of overlap between the histograms is highest for the standard B-mode image, whereas there is no overlap for the cubic image. Comparison with the histograms resulting from the quadratic image, cubic image histograms exhibit virtually complete separation

Further insight into the workings of the ThOVF can be obtained by examining the average spectra of data from the UCA and tissue region. These results are shown in Fig. 4 where the UCA spectra are shown in dark solid line while the tissue spectra are shown in lighter solid line. It is interesting to see that the PI data shows significant enhancement at the fundamental indicating that the contrast enhancement is (at least in part) due to the motion of the contrast agent in the flow channel. Much smaller enhancement at the second harmonic can be observed from the PI spectra. On the other hand, the quadratic and cubic components show spectral peaks at frequencies predicted by the theory of quadratic and cubic filters. Specifically, low-frequency and 2nd harmonic for the quadratic filter and fundamental and 3rd harmonic for the cubic filter. In addition, spectra from the cubic data show a significantly larger degree of separation between UCA and tissue data.

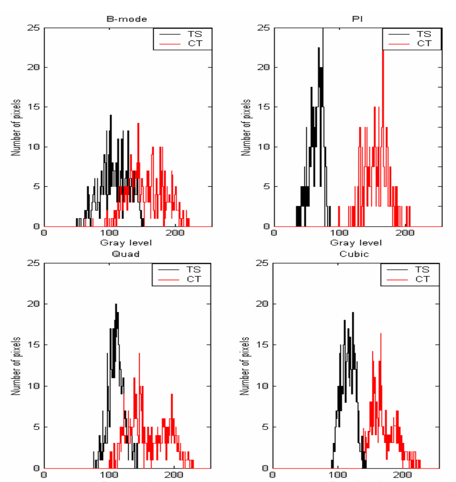

Fig. 3 Gray-level histograms produced from images shown in Fig. 2. Histograms are produced from the contrast region (lighter) and the tissue region (darker).

5. CONCLUSIONS

Results have shown that the application of the ThOVF to pulse-echo ultrasonic data from imaging tissue and UCAs is effective in the separation of the nonlinear echoes from those regions. Thus it is possible to maximize the contrast between these regions without loss of spatial resolution. In addition, compared to PI imaging, the VF approach does not require multiple transmissions for acquiring one image line. Therefore, this approach preserves the frame rate of the original B-mode system, an important advantage of ultrasound imaging over other medical imaging modalities.

6. REFERENCES

[1] K. I. Kim and E. J. Powers, "A digital method of modeling quadratically nonlinear systems with a general random input," *IEEE Trans. Acoust., Speech, Signal Processing,* vol. 36, no. 11, pp. 1758-1769, Nov. 1988.

[2] T. Koh and E. J. Powers, "Second-order volterra filtering and its application to nonlinear system identification," *IEEE Trans. Acoust., Speech, Signal Processing,* vol. ASSP-33, no. 6, pp. 1445-1455, Dec. 1985.

[3] H. Yao, P. Phukpattaranont, and E. S. Ebbini, "Post-beamforming second-order Volterra filter for nonlinear pulse-echo imaging," *ICASSP,* pp. 1133-1136, 2002.

[4] J. Ophir and K. J. Parker, "Contrast agent in diagnostic ultrasound," *Ultrasound in Med. & Biol.,* vol. 15, no. 4, pp. 319-333, Nov. 1989.

[5] D. H. Simpson, C. T. Chin, and P. N. Burns, "Pulse inversion Doppler: A new method for detecting nonlinear echoes from microbubble contrast agent," *IEEE Trans. Ultrason., Ferroelect., Freq. Contr.,* vol. 46, no. 2, pp. 372-382, Mar. 1999.

[6] P. Phukpattaranont and E. S. Ebbini, "Post-beamforming second-order Volterra filter for nonlinear pulse-echo ultrasonic imaging," *IEEE Trans. Ultrason., Ferroelect., Freg. Contr*., vol. 50, no. 8, pp. 987-1001, Aug. 2003.

[7] P. Phukpattaranont, M. F. Al-Mistarihi and E. S. Ebbini, 'Post-beamforming Volterra filters for contrast-assisted ultrasonic imaging: In-vivo results," in *Proc. IEEE Ultrason. Symp*., 2003.

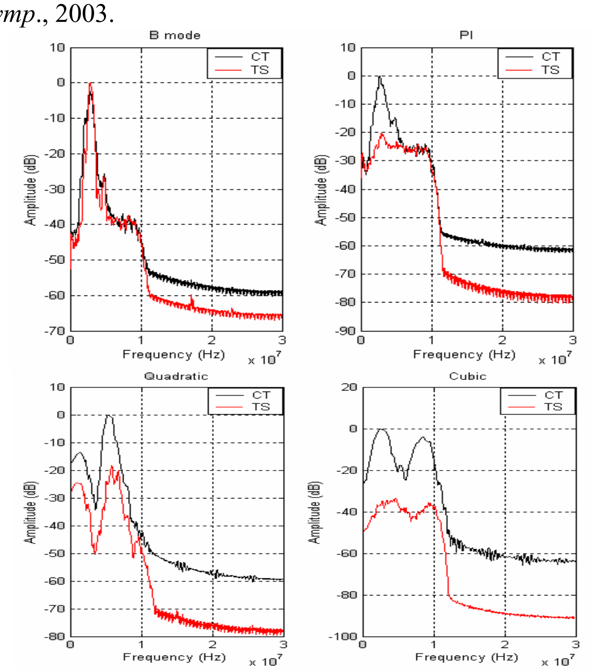

Fig. 4 Average spectra from the contrast (darker) and tissue (lighter) of the flow phantom: Standard B-mode, PI, Quadratic, and Cubic.